TU Delft

Delft University of Technology

Document Version
Final published version

Licence
CC BY

Citation (APA)
Umans, S. A., de Vos, B., Harder, B. M., Gutknecht, J., Watson, S. J., & van Wingerden, J. W. (2026). An actuatable porous disk for miniature active cluster wake control windtunnel experiments. *Journal of Physics: Conference Series*, *3224*, Article 032026. https://doi.org/10.1088/1742-6596/3224/3/032026

Important note
To cite this publication, please use the final published version (if applicable).
Please check the document version above.

Copyright
In case the licence states “Dutch Copyright Act (Article 25fa)”, this publication was made available Green Open Access via the TU Delft Institutional Repository pursuant to Dutch Copyright Act (Article 25fa, the Taverne amendment). This provision does not affect copyright ownership.
Unless copyright is transferred by contract or statute, it remains with the copyright holder.

Sharing and reuse
Other than for strictly personal use, it is not permitted to download, forward or distribute the text or part of it, without the consent of the author(s) and/or copyright holder(s), unless the work is under an open content license such as Creative Commons.

Takedown policy
Please contact us and provide details if you believe this document breaches copyrights.
We will remove access to the work immediately and investigate your claim.

This work is downloaded from Delft University of Technology.

Journal of Physics:
Conference Series

PURPOSE-LED
PUBLISHING™

PAPER • OPEN ACCESS

An actuatable porous disk for miniature active cluster wake control windtunnel experiments

To cite this article: S.A. Umans *et al* 2026 *J. Phys.: Conf. Ser.* **3224** 032026

View the article online for updates and enhancements.

You may also like

- The Apache Point Observatory Lunar Laser-ranging Operation: Instrument Description and First Detections
T. W. Murphy, E. G. Adelberger, J. B. R. Battat et al.
- A high-speed single-photon detection scheme based on frequency domain filtering
Jin Wu, Yue Rong, Chenggong Wan et al.
- Assessment of absorbed power density and temperature rise for nonplanar body model under electromagnetic exposure above 6 GHz
Yinliang Diao, Essam A Rashed and Akimasa Hirata

This content was downloaded from IP address 131.180.130.31 on 18/08/2026 at 13:09

Journal of Physics: Conference Series **3224** (2026) 032026 doi:10.1088/1742-6596/3224/3/032026

An actuatable porous disk for miniature active cluster wake control windtunnel experiments

S.A. Umans[1], B. de Vos[1], B.M. Harder[1], J. Gutknecht[1], S.J. Watson[2] and J.W. van Wingerden[1]

[1]Delft Center for Systems and Control, Delft University of Technology, Delft, The Netherlands

[2]Flow Physics and Technology, Delft University of Technology, Delft, The Netherlands

E-mail: s.a.umans@tudelft.nl

Abstract. An actuatable porous disk (APD) with controllable porosity is presented, with the purpose of enabling future turbine cluster experiments on a small scale with dynamic collective induction control. Here, a proof of concept for the APD model is presented, including analyses of both static and dynamic behavior. To quantify the wake, the APD wake is probed with a static sensor porous disk placed at various positions in the wake. The results show that the APD thrust coefficient is strongly correlated to the porosity, and the unsteady spectrum of the wake contain clear peaks at APD actuation frequencies. This proves the capabilities of the APD model for dynamically controlling its thrust coefficient and altering its wake.

1. Introduction

The physics of wind turbine wake interactions has been recognized as an open field of research for the past decade [1]. On a larger scale, losses resulting from inter-farm cluster wake effects are drawing attention from the scientific community and the wind energy industry. Finserås et al. [2] note that under certain atmospheric conditions, cluster-wake-induced power losses in downwind farms are significant and that these losses have been underestimated. As a possible solution, the turbine cluster can be controlled with the purpose of increasing cluster wake recovery through dynamic collective induction control, similar to active wake mixing on the turbine-to-turbine scale. This method, named active cluster wake control (ACWC) [3, 4], has the potential to increase annual energy production of currently operating wind farms, with no necessary mechanical changes to the existing turbines, though this needs extensive validation.

One hurdle in the development of ACWC methods is the large length- and timescale of the problem, typically spanning domains of tens of kilometers with advection timescales of up to an hour. A tool for early investigations of cluster actuation methods that could quickly make a rough assessment of the performance of these methods would be valuable for the progression of this research field.

Two ways to explore the potential for cluster actuation are numerical simulation and wind tunnel experimentation. Numerically evaluating ACWC methods through large eddy simulations with appropriately sized domains is slow and computationally expensive [5], and no validated dynamic engineering models exist for the far farm wake. Alternatively, scaled wind tunnel experiments could facilitate relatively quick assessment. These experiments require scaled models, sufficiently small to fit in regular wind tunnels. Scale models fit into two categories: bladed

Content from this work may be used under the terms of the Creative Commons Attribution 4.0 licence. Any further distribution of this work must maintain attribution to the author(s) and the title of the work, journal citation and DOI.
Published under licence by IOP Publishing Ltd

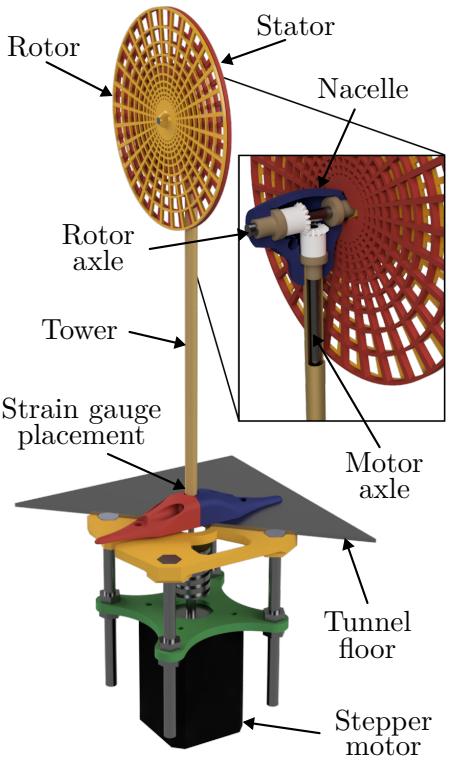

Figure 1. Model render with internal nacelle details.

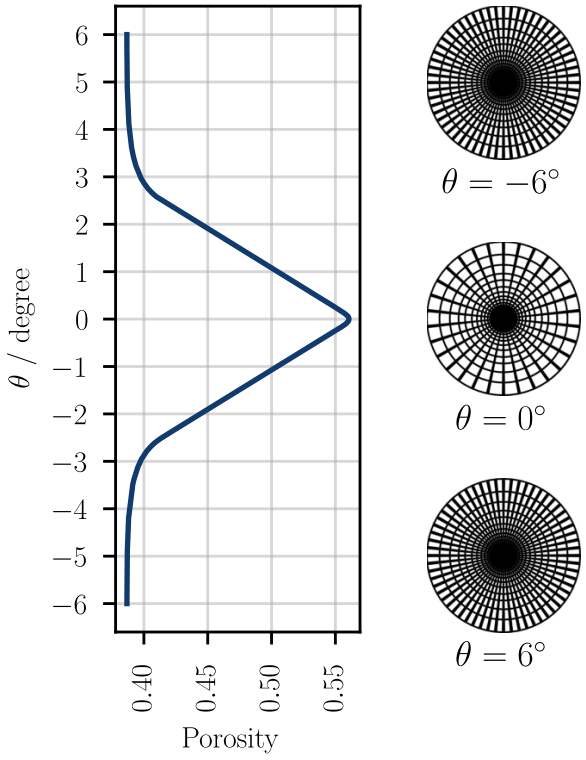

Figure 2. Theoretical porosity curve as a function of angular offset, with the corresponding extreme and zero position frontal faces depicted on the right.

turbines, and Porous Disks (PDs). Small bladed turbines require a high-precision electro-motor and controller board, complicating the scaling to large farm setups. Conversely, PDs are more suitable to scale to large farm setups, as shown in Messmer et al. [6].

Additionally, a PD with the purpose of assessing ACWC methods should have a variable thrust coefficient. De Vos et al. [7] have demonstrated that for PDs, porosity variations are able to dynamically alter the wake, and show a relatively high control bandwidth. Another example of such an Actuatable Porous Disk (APD) is presented in Yu et al. [8] where the disk has a uniformly distributed porosity. This APD with a rotor diameter of 60 cm is too large for farm scale experiments, where static farm scale rotor diameters are generally between 4.5 cm [9] and 12 cm [6]. The mechanisms used for the APD by Yu et al. are difficult to scale down to the required sizes for farm setups, making the APD unsuitable for these purposes.

A new APD model is therefore developed, allowing practical scalability of the number of turbines in a wind tunnel. This paper aims to validate the concept of this scale model that will be introduced in Sec. 2. This validation enables future use of the APD to perform wind tunnel experiments of collective control in wind farms. To summarize, the APD model is required: (i) to have controllable induction and be able to alter the wake, (ii) to be small enough for a large farm setup in a regular tunnel, (iii) to be scalable to a large farm setup.

2. Method

In this section, the mechanical and electrical design of the proposed APD model is explained in Sec. 2.1. Then, in Sec. 2.2, the calibration campaign is defined, as well as the main experiment.

2.1. Model Description

2.1.1. Mechanical System Since aerodynamic thrust is coupled to PD porosity, the key feature of the APD is that it has variable porosity, as shown in Fig. 2. This mimics a change in turbine rotor thrust by varying the fraction of the flow which can pass through the disk. This is achieved by having two stacked porous disks, where the rear disk (stator) is fixed to the nacelle and the front disk (rotor) is connected to a stepper motor. This motor is placed underneath a wind tunnel and connects to the rotor through a miter gear in the nacelle. The nacelle is mounted on a tower which is rigidly fixed to the floor of the wind tunnel used for testing. A render of the model is shown in Fig. 1, where the stator is colored red and the rotor yellow. Also indicated are the placements of the strain gauges at the tower base that measure the tower base strain induced by the aerodynamic thrust force.

The geometry of the porous disks is taken from Camp and Cal [10] and truncated to a 10 cm diameter. As shown in Fig. 2, it is a nonuniform PD, as opposed to the uniform APD presented by Yu et al. [8]. The design by Camp and Cal has been thoroughly tested by Aubrun et al. [11] in a round-robin test and has been used for other wind farm wind tunnel experiments in Messmer et al. [6]. The truncated disk geometry consists of 10 concentric, and 30 equispaced radial ribs. This results in an angular offset, θ, limit of $\frac{360^\circ}{30} = 12^\circ$ between the stator and rotor, before axial symmetry occurs between offsets.

The porosity of the APD only decreases with increasing angular offset as long as the radial ribs of the rotor partially overlap. As long as this partial overlap exists, the frontal surface area of the combined disks can increase and therefore the porosity decreases. When the partial overlap disappears for $|\theta| \gtrsim 3.25^\circ$, the frontal area does not increase any more and the porosity stays constant, as depicted in Fig. 2.

Both the PDs and the nacelle are fabricated using consumer-grade 3D-printing, where the PDs are made through fused filament fabrication and the nacelle is made with stereolithography. The nacelle houses the flanged bushings aligning the rotor and tower axles, and the miter gears coupling the rotor axle to the tower axle. Backlash in the miter gears can be minimized by slightly compressing the flexible motor coupling connecting the motor axle to the tower axle, such that the gearing is also under slight compression.

Since there is no gear ratio between the stepper motor and rotor, the resolution of the stepper motor equals the porosity resolution of the APD. The stepper motor used here (JKONGMOTOR JK42HM60-1684A-03F) has a full step size of 0.9° and the stepper motor driver (DRV8825) allows for 32 intermediate microsteps per full step, resulting in a step size of $2.8 \cdot 10^{-2\,\circ}$ and therefore 426 discrete angles to control the porosity in the range $\theta \in [0^\circ, 12^\circ]$.

To measure the wake created by the APD, a Sensor Porous Disk (SPD) of the same diameter, but with fixed porosity and radial ribs of twice the thickness, is also equipped with strain gauges [7]. This SPD is mounted on a large, heavy, and rigid steel base to allow it to be located at varying positions in the wake, instead of being fixed to the wind tunnel floor. How this SPD measures the wake is described in more detail in Sec. 2.2.

2.1.2. Electrical System The actuation and acquisition system was built in-house and runs on a single ESP32-S3 microcontroller. The actuation controller drives the stepper motor to allow a predetermined rotational movement of the APD rotor. The zero position of the rotor is manually offset by adjusting a potentiometer, allowing alignment of the radial ribs of the rotor and stator.

The acquisition circuitry consists of a Wheatstone half-bridge, two amplifiers, an analog antialiasing filter, and an analog to digital converter (ADC), yielding a sampling frequency of 125 Hz. This signal chain is summarized in Fig. 3. Firstly, the bending of the tower due to the PD thrust force causes an elongation of the strain gauges (HBK 1-LY63-3/350) at the tower base. This results in an imbalance in the Wheatstone bridge, causing a small voltage difference.

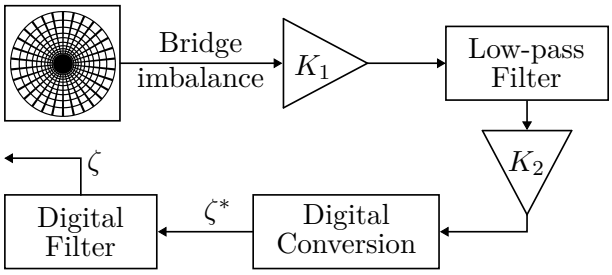

Figure 3. Summary of the acquisition signal chain, starting from the bridge imbalance caused by the strain gauges elongation.

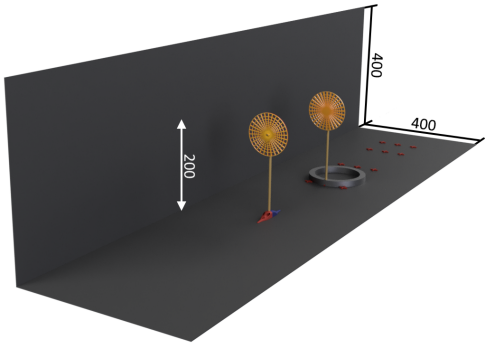

Figure 4. Tunnel, APD, SPD, and red SPD placement markers to scale.

This voltage difference is amplified with a gain $K_1 = 727$ (AD620 board). The amplified signal is then passed through an analog 4th order Butterworth type antialiasing filter (Krohn-Hite model 3945) with a cutoff frequency set to 40 Hz. This signal goes to a 16-bit ADC with built-in pre-conversion amplifier (ADS1115 board). This amplifies the filtered signal again with a gain $K_2 = 16$ before digitizing it and passing it to the microcontroller, i.e. the tower base strain $\epsilon \in [-2^{15}, 2^{15}]$. Finally, a digital filter may be applied to filter out tunnel resonances.

Collectively, the bridge imbalance voltage is amplified by a factor of 11632, and since the logic voltage for the ADC is 3.3 V, this yields an analog signal range of ± 0.14 mV. The digital voltage measurements, ζ, will be presented normalized on the digital measurement range, i.e. $\zeta = \frac{\epsilon}{2^{16}} \in [-0.5, 0.5]$. This normalized measure has a resolution of $1.5 \cdot 10^{-5}$, corresponding to 4.3 nV at the bridge.

2.2. Experimental Design

2.2.1. Wind Tunnel Description The wind tunnel used for testing has a closed return flow with an outflow contraction ratio of 38%, and a honeycomb flow straightener at the inflow. It has a maximum center flow speed of 6 m/s and a test cross-section of 400 mm by 400 mm, as depicted in Fig. 4. The blockage ratio of one solid-disk APD is therefore 5%. Lastly, the PDs are placed in the center flow of the tunnel, resulting in a PD hub height of 200 mm.

2.2.2. Calibration Campaign Firstly, the digital filter is tuned to reject tunnel and tower resonances. These resonance frequencies are determined from the impulse responses, where the impulse is given at the tunnel fan section and the PD nacelles. Secondly, a measurement of the system at rest gives an impression of the ambient noise generated by the system.

Furthermore, two characteristic parameters have to be estimated from calibration measurements for each PD. These are the tower stiffnesses and the thrust coefficient curves of both the APD and the SPD. The tower stiffness, J, may be determined through the linear relationship, $\epsilon = JT$, between induced strain, ϵ, and aerodynamic thrust, T. This stiffness parameter J is estimated by mounting the PDs horizontally and setting varying calibration weights in the rotor center. A linear least squares (LLS) fit then yields the estimate and its uncertainty.

For the thrust coefficients, the relationship

$$T = \frac{1}{2}\rho\pi\left(\frac{1}{2}D\right)^2 C_T u_\infty^2 = \kappa C_T u_\infty^2 \tag{1}$$

is obtained from momentum theory, where ρ is the air density, D is the PD diameter, C_T is the thrust coefficient and varies with the porosity [12], u_∞ is the free stream velocity, and

$\kappa = \frac{1}{8}\rho\pi D^2$. Substitution yields

$$\epsilon = \kappa J C_T u_\infty^2. \tag{2}$$

Because the C_T of the SPD, C_T^{S}, is constant, it is possible to reconstruct the rotor effective free stream velocity, u_r^{S}, as

$$u_r^{\mathrm{S}} = \sqrt{\frac{\epsilon}{\kappa J^{\mathrm{S}} C_T^{\mathrm{S}}}}. \tag{3}$$

The SPD thrust coefficient is estimated as the nonlinear least squares (NLS) solution to Eq. 2 with varying free stream velocities. The APD thrust coefficient, C_T^{A}, is dependent on θ, however. Therefore, it is obtained from the NLS solution of Eq. 2, with u_∞ fixed at 5 m s^{-1} and varying values of θ. The curve that is fitted to the calibration data is linear in the overlapping range and constant in the constant porosity range, i.e.

$$C_T^{\mathrm{A}}(\theta) = \begin{cases} c_0, & |\theta| >= 3.25, \\ c_1|\theta| + c_0 - 3.25c_1, & |\theta| < 3.25, \end{cases} \tag{4}$$

2.2.3. Experimental Campaign For the main experiment, the APD is actuated at four distinct frequencies, $f \in \{0.5, 1, 2, 3\}$ Hz, with a free stream velocity of 5 m s^{-1}. These actuation signals are defined as $\theta(t) = \Gamma \sin(2\pi f t) + \gamma$. The choice of these frequencies is motivated by the ACWC method presented by Gutknecht et al. [3], which would result in an oscillation of 2 Hz in a 1 m wide wind farm for 5 m s^{-1} inflow.

During this actuation, the SPD measurements are collected at various positions in the wake. These positions are placed on the regular grid $X_{\mathrm{SPD}} \times Y_{\mathrm{SPD}} = \{3D, 5D, 7D, 8D\} \times \{-D/2, 0, D/2\}$, as shown by the markers in Fig. 4. From these measurements, the SPD rotor effective free stream velocity is reconstructed through Eq. 3.

These measurements are compared on the steady, $\bar{u}_r^{\mathrm{S}}$, and unsteady, $\tilde{u}_r^{\mathrm{S}}$, parts of the Reynolds decomposition. The frequency spectrum of the unsteady timeseries should show whether the actuation of the APD alters the wake. This spectrum is smoothed using Welch's method of estimating the spectrum of the measurement.

The steady parts of the measurements are obtained by taking the time average of the measurement series. These values are then compared to the algebraic far wake model presented by Bastankhah and Porté-Agel [13],

$$\frac{U_w^{\mathrm{A}}}{u_\infty} = \sqrt{1 - \frac{C_T^{\mathrm{A}}}{8\left(0.0175x' + 0.1\frac{1+\sqrt{1-C_T^{\mathrm{A}}}}{\sqrt{1-C_T^{\mathrm{A}}}}\right)^2}}\; e^{y^2\left(-2D\left(0.0175x' + 0.1\frac{1+\sqrt{1-C_T^{\mathrm{A}}}}{\sqrt{1-C_T^{\mathrm{A}}}}\right)\right)^{-2}} \tag{5}$$

at hub height for a turbulence intensity of 5%, where $x' = x/D$.

3. Results and Discussion

In this section, the results of the calibrations and experiments are shown and interpreted, and any remarkable findings are discussed. First, the calibration results are presented in Sec. 3.1. Then the results of the experiments with dynamic actuation are presented in Sec. 3.2. Lastly, some remarks are made on the acquisition system in Sec. 3.3 and improvements to the model are suggested in Sec. 3.4.

Table 1. Parameter values, or estimations and confidence intervals.

Parameter	Value	Unit	Standard deviation	95% CI
J^{A}	$7.75{\cdot}10^{-1}$	N^{-1}	$5.15{\cdot}10^{-3}$	$[7.65{\cdot}10^{-1}, 7.85{\cdot}10^{-1}]$
J^{S}	$7.69{\cdot}10^{-1}$	N^{-1}	$7.39{\cdot}10^{-3}$	$[7.55{\cdot}10^{-1}, 7.84{\cdot}10^{-1}]$
C_T^{S}	$8.70{\cdot}10^{-1}$	-	$2.63{\cdot}10^{-2}$	$[8.17{\cdot}10^{-1}, 9.22{\cdot}10^{-1}]$
c_0	$6.96{\cdot}10^{-1}$	-	$2.41{\cdot}10^{-2}$	$[6.48{\cdot}10^{-1}, 7.45{\cdot}10^{-1}]$
c_1	$4.42{\cdot}10^{-2}$	$\circ^{-1}$	$4.02{\cdot}10^{-3}$	$[3.62{\cdot}10^{-2}, 5.23{\cdot}10^{-2}]$
κ	$4.87{\cdot}10^{-3}$	$\mathrm{kg\ m}^{-1}$	-	-
Γ	1.5	$\circ$	-	-
γ	1.5	$\circ$	-	-

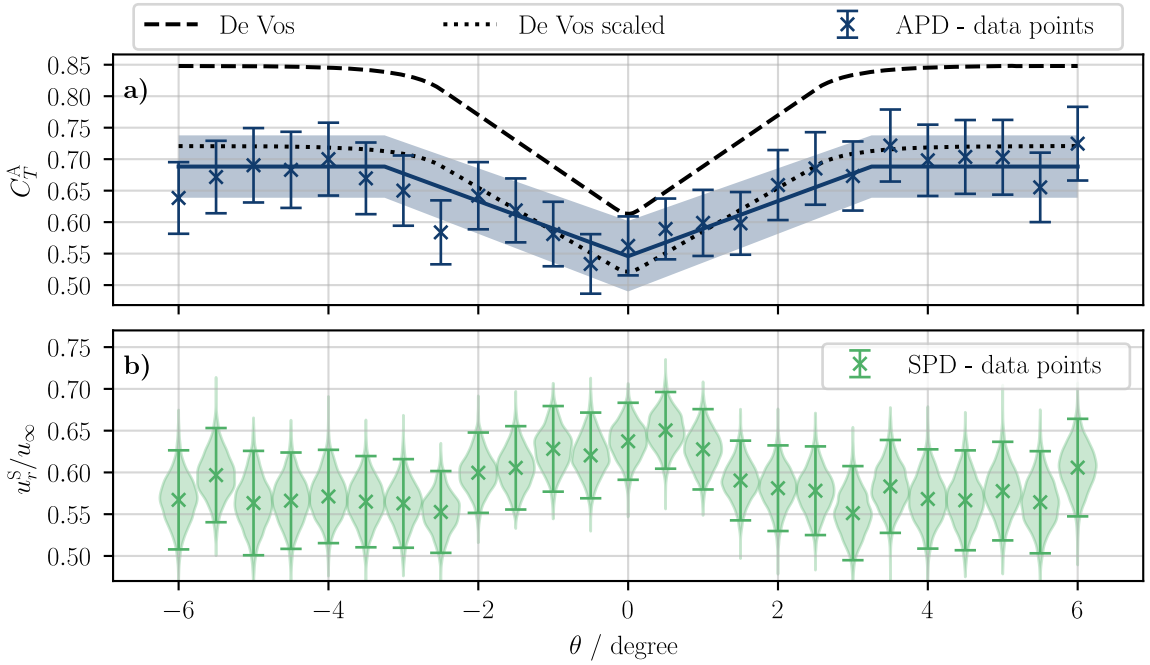

Figure 5. a) APD thrust coefficient calibration as a function of angular offset, with the estimated curve-fit and the parameter estimate uncertainty confidence interval. Also shown is the porosity-C_T relation proposed by De Vos et al. and an 85% scaling of this [7]. **b)** The respective velocity measurements of the SPD, placed $3D$ downstream, are plotted as violin plots. All data point whiskers indicate the 95% CI of the measured timeseries.

3.1. Parameter Calibration

Three calibration measurements were performed to obtain: (i) the tower stiffnesses, (ii) the SPD thrust coefficient, and (iii) the APD thrust coefficient curve (Fig. 5). The estimated parameters are tabulated in Table 1. Furthermore, the measurement of the system at rest resulted in a sample of the ambient noise on the output ζ^*, which is high frequency noise with a maximum amplitude of 10^{-3}. For the second and third calibrations, the measurements were digitally filtered. The digital filter was set to an 8th order Butterworth low-pass filter with a 10 Hz cutoff frequency to remove the tunnel and tower resonances. From the measured impulse responses, it was determined that any tunnel or tower resonances lie above 15 Hz and the largest disturbances occur around 32 Hz.

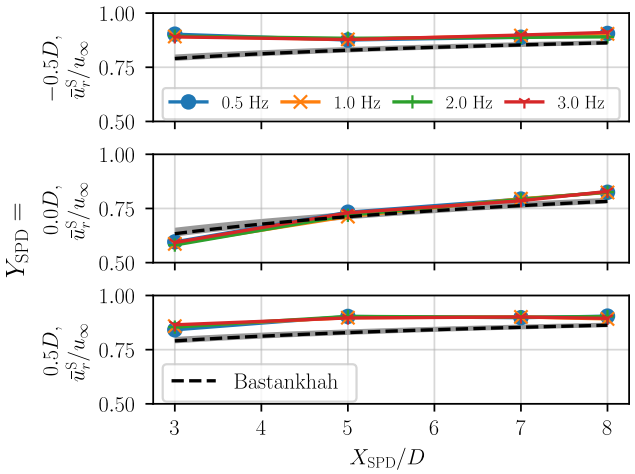

Figure 6. The mean SPD velocity measurements at different positions in the wake compared to the expected wake from Bastankhah's model for a turbulence intensity of 5%. The model lines correspond to $\theta = \gamma$ and the shaded areas around are the images of $\theta \in \gamma \pm \Gamma$.

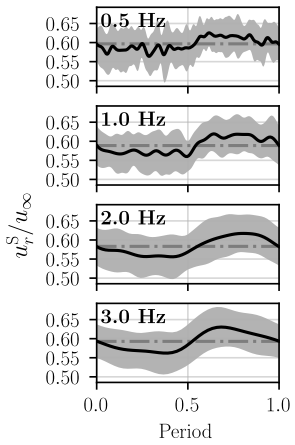

Figure 7. Phase average with the SPD placed in the center wake and $3D$ downstream.

Firstly, the two LLS to obtain the tower stiffnesses resulted in excellent fits with $R^2 = 1.00$ for both PDs and 95% confidence intervals (95CIs) of less than ±2% on the estimated stiffnesses. Secondly, the NLS for Eq. 2 and the measurements at varying wind speeds resulted in a reasonable C_T^{S} estimate, with $R^2 = 0.897$ for the fit and a ±6% 95CI on the estimated value. Lastly, the model in Eq. 4 fits the measurements to an acceptable degree, with $R^2 = 0.745$ and 95CIs of ±7% and ±18% for c_0 and c_1, respectively. Qualitatively, however, the trend seems to be captured well with the exception of the outlier at $\theta = -2.5°$, as seen in Fig. 5, and follows the porosity trend shown in Fig. 2. The fit results in a codomain $C_T^{\mathrm{A}}(\theta) \in [0.55, 0.7]$, which is a reasonable range of operation and in agreement with the static C_T value found by Camp and Cal [10]. Furthermore, the SPD velocity measurements from $3D$ downstream of the APD, shown in the bottom plot of Fig. 5, correlates with the inverse of the $C_T^{\mathrm{A}}(\theta)$ trend. This shows that higher $C_T^{\mathrm{A}}(\theta)$ values do incur a stronger wake deficit.

Also plotted in Fig. 5 is the thrust coefficient model as proposed by De Vos et al. [7]. This is a linear model derived from a meta-analysis and is defined as $C_T = -1.35p + 1.37$ with p being the porosity. Although this model is similar in shape to the data and found fit, there is a scaling disagreement of roughly 15%. Applying this heuristic correction does cause the model to fall in the 95CI of the current fit over the full range.

3.2. Dynamic Actuation Trials

The SPD measurements for the different SPD positions and APD actuation frequencies are split in two parts. The mean part is depicted in Fig. 6 and the estimated spectrum of the unsteady part is shown in Fig. 8. Furthermore, the phase average of the actuation period of each frequency is shown in Fig. 7.

The steady SPD velocity measurements are depicted in Fig. 6. This graph shows a wake and its recovery across all measurements along the wake center. The outer edge measurements show a much weaker version of the same trend. Furthermore, the means of all individual SPD positions agree for different frequencies, indicating a high consistency between trials.

Compared to the wake model described in Sec. 2, the measurements agree well with the far wake model proposed by Bastankhah and Porté-Agel [13] with an overall fit of $R^2 = 0.856$ to the

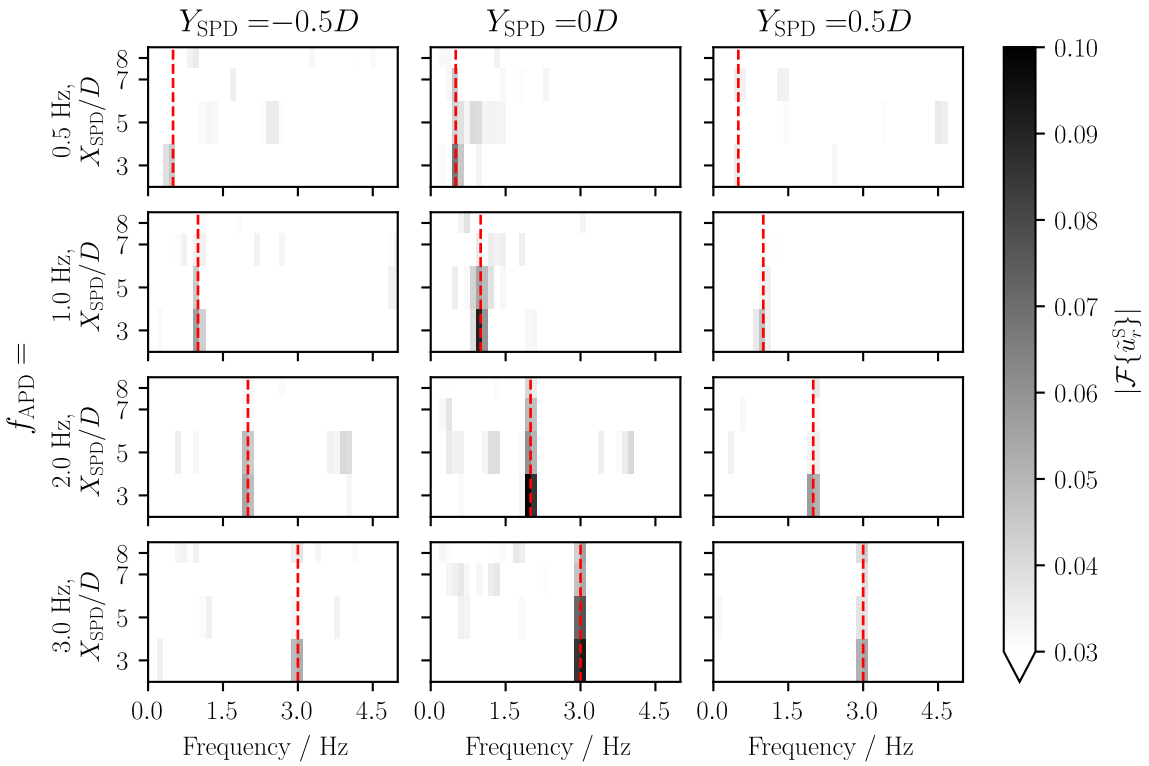

Figure 8. Fourier transforms of the unsteady SPD measurement components for different APD actuation frequencies at different positions in the wake. The red dashed lines indicate the APD actuation frequency.

ensemble average of all frequencies in the center wake. For the off-center SPD positions, it seems however that there are accelerations, likely due to the nearness of the tunnel walls ($1D$ disk-edge to wall distance). The restricted wake expansion most likely also causes an artificially increased wake recovery, perhaps explaining the slight measurement deviation from Bastankhah's model observed 7 and $8D$ downstream in the center wake.

The phase averages depicted in Fig. 7 show qualitatively good agreement of the wake response to the different actuation frequencies. It must be noted that these averages were derived from fixed-length measurements and not fixed-periods measurements. The number of sample periods is therefore 24, 48, 96, and 144 for 0.5, 1, 2, and 3 Hz actuation, respectively. This is likely to account for some of the roughness in the averages for lower frequencies. On the other hand, the 95CI of all averages are similar in magnitude, opposing the notion that more samples should decrease the uncertainty. It can therefore be argued that the shown average uncertainty has a different origin and that it dominates the uncertainty induced by the actuation. This is further supported by the observation that the 95CI shown in Fig. 7 and the SPD velocity measurements shown in Fig. 5 have a similar magnitude, whilst the first results from dynamic APD actuation and the latter from static cases.

The spectra of the unsteady part of the measurements are shown in Fig. 8. The center wake shows clear peaks at the actuation frequencies, indicating that the wake is altered by the dynamic actuation. However, the lower the frequency, the faster this perturbation diffuses as the wake is advected downstream. This trend is less apparent in the outer position measurements, where all frequencies diminish at roughly the same rate.

3.3. On the Acquisition System

The measurement of the system at rest indicates that there is roughly 10^{-3} amplitude random ambient noise on the measurements in any case. This means that the 6 least significant bits of the 16 bit digital ϵ-signal are disregardable. Another consideration is to actually decrease the amount of noise coming from the strain gauges. The wires connecting the strain gauges have been found to be highly susceptible to external electrical fields, generated by for example the stepper motor or the wind tunnel fan motors. Lastly, the sampling rate of 125 Hz was sufficient for performing the currently presented experiments and to draw conclusions on the proof of concept. However, with the end goal in mind to operate larger clusters of APDs, this sampling rate is not sufficient to scale to multiple APDs, since the number of samples per second is shared amongst all APDs.

3.4. Suggested Improvements

There are three suggested improvements to the model based on the presented tests. First is the reduction of ambient noise. By placing the first amplifiers as close to the strain gauges as possible, keeping the wires as short as possible, and twisting and shielding them, the noise levels at rest should be significantly reduced. Overall, this increases the achievable resolution and improves the measurement quality.

Secondly, since the current measurements are sufficient for identifying the actuation effects in the wake, a 10-bit discretization of the measured analogue signal is fine enough with this amplification. This makes the dedicated 16 bit ADC redundant, because the ESP32-S3's built-in 12 bit ADC should suffice. This ADC has a much higher sampling rate of 200 kHz shared amongst 20 channels, theoretically allowing for a 10 kHz sampling rate for a 20 APD configuration on a single microcontroller.

Lastly, the nacelle construction can be improved on two main points. These are further removing backlash from the miter gear coupling by improving the axle alignments, and making the connection between the nacelle and the tower more rigid in the tower-axial direction. For these experiments, care was taken to always approach θ-setpoints from a single direction. To ensure the rigidity of the nacelle attachment, an extra set screw (not shown in Fig. 1) was added to clamp onto the tower.

4. Conclusions

A proof of concept of an APD with variable porosity is presented to enable wind tunnel experiments of large clusters of turbines performing dynamic thrust control. The results show that the APD model succeeds in actuating the wake both statically and dynamically. It was demonstrated that the thrust coefficient of the APD is strongly correlated to the porosity. Furthermore, unsteady perturbations in the wake have been shown at the same frequencies as the actuation, indicating that the model is capable of dynamically actuating the wake.

To further validate the suitability of this model for farm actuation assessment, inquiries should be made into the similarity between cluster wakes of arrays of APDs and full scale cluster wakes. Attention should be given to the far wakes of these clusters and how responsive these are to dynamic actuation.

Lastly, all resources necessary to replicate the presented APD are provided in [14].

Acknowledgements

This research received funding from TKI Offshore, under grant "TKITOE WOZ 2403 TUD CLUSTERWAKE". Much gratitude is owed to the laboratory technicians of the Delft Center for

Systems and Control for their support in the development of this model.

References

[1] Meyers J, Bottasso C, Dykes K, Fleming P, Gebraad P, Giebel G, Göçmen T and van Wingerden J W 2022 Wind farm flow control: prospects and challenges *Wind Energy Science* **7** 2271–2306 ISSN 2366-7443 publisher: Copernicus GmbH

[2] Finserås E, Herrera Anchustegui I, Cheynet E, Gebhardt C G and Reuder J 2024 Gone with the wind? Wind farm-induced wakes and regulatory gaps *Marine Policy* **159** 105897 ISSN 0308-597X

[3] Gutknecht J, Becker M, Taschner E, Stipa S, Allaerts D, Viré A and van Wingerden J W 2024 Active Cluster Wake Mixing *Journal of Physics: Conference Series* **2767** 092052 ISSN 1742-6596 publisher: IOP Publishing

[4] Gutknecht J, Taschner E, Becker M, Viré A and Wingerden J W V 2025 Mitigating cluster wake induced power losses at neighboring wind farms through cluster-wide coordinated control

[5] Stipa S, Ajay A, Allaerts D and Brinkerhoff J 2024 TOSCA – an open-source, finite-volume, large-eddy simulation (LES) environment for wind farm flows *Wind Energy Science* **9** 297–320 ISSN 2366-7451

[6] Messmer T, Centurelli G, Wagner M, Umdenstock H, Peinke J and Hölling M 2025 From single turbine to wind farm wake: a wind tunnel study *Journal of Physics: Conference Series* **3016** 012009 ISSN 1742-6596

[7] De Vos B, Harder B M, Huisman T A, Gutknecht J and Van Wingerden J W 2024 Mimicking the Helix with a porous disc for wind tunnel testing *Journal of Physics: Conference Series* **2767** 092063 ISSN 1742-6588, 1742-6596

[8] Yu W, Hong V W, Ferreira C and van Kuik G A M 2017 Experimental analysis on the dynamic wake of an actuator disc undergoing transient loads *Experiments in Fluids* **58** 149 ISSN 1432-1114

[9] Vinnes M K, Neunaber I, Lykke H M H and Hearst R J 2023 Characterizing porous disk wakes in different turbulent inflow conditions with higher-order statistics *Experiments in Fluids* **64** 25 ISSN 0723-4864, 1432-1114

[10] Camp E H and Cal R B 2016 Mean kinetic energy transport and event classification in a model wind turbine array versus an array of porous disks: Energy budget and octant analysis *Physical Review Fluids* **1** 044404

[11] Aubrun S e 2019 Round-robin tests of porous disc models *Journal of Physics: Conference Series* **1256** 012004 ISSN 1742-6588, 1742-6596

[12] Lignarolo L E M, Ragni D, Ferreira C J and Van Bussel G J W 2016 Experimental comparison of a wind-turbine and of an actuator-disc near wake *Journal of Renewable and Sustainable Energy* **8** 023301 ISSN 1941-7012

[13] Bastankhah M and Porté-Agel F 2014 A new analytical model for wind-turbine wakes *Renewable Energy* **70** 116–123 ISSN 09601481

[14] Umans S 2025 4TU.ResearchData repository "Actuatable Porous Disk - Fabrication and Data"